Finite-Temperature Monte Carlo Calculations for Systems with Fermions

Shiwei Zhang
Department of Applied Science and Department of Physics, College of William and Mary, Williamsburg, Virginia 23187
(Received 18 November 1998)

We present a quantum Monte Carlo method which allows calculations on many-fermion systems at finite temperatures without any sign decay. This enables simulations of the grand-canonical ensemble at large system sizes and low temperatures. Both diagonal and off-diagonal expectations can be computed straightforwardly. The sign decay is eliminated by a constraint on the fermion determinant. The algorithm is approximate. Tests on the Hubbard model show that accurate results on the energy and correlation functions can be obtained.

PACS numbers: 71.10.Fd, 02.70.Lq, 74.20.–z

The quantum Monte Carlo method for simulating grand-canonical ensembles, originally formulated by Blankenbecler, Scalapino, and Sugar (BSS) [1], is widely applied in areas spanning condensed-matter, high-energy, and nuclear physics. The method allows essentially exact calculations of finite-temperature equilibrium properties of interacting fermion systems. It expresses the partition function as a many-dimensional integral over a set of random auxiliary fields. The many-dimensional integral is then computed by Monte Carlo (MC) techniques.

As all current fermion quantum Monte Carlo methods, however, the BSS algorithm suffers from the well-known sign problem [2,3]. The integrand of the partition function is not all positive. Indeed its average sign approaches zero as the temperature is lowered. As a result, contributions from the Monte Carlo samples largely cancel. The partition function, which is given by the difference between the positive and the negative, becomes a vanishingly small quantity compared to the MC noise. The computational cost for fixed statistical accuracy scales exponentially with system size and inverse temperature. While for many problems the BSS algorithm is the most, sometimes *only*, feasible approach, the sign problem has remained completely uncontrolled in the algorithm. This has severely limited the temperatures and sizes accessible and has prohibited studies of a variety of interesting problems in correlated systems, particularly concerning true phase transitions.

In this Letter, we present a finite-temperature method which is free of any decay of the average sign and which retains many of the advantages of the BSS formalism, thus allowing grand-canonical calculations at lower temperatures and larger system sizes with favorable scaling. Below we first derive a set of *exact* constraints on the auxiliary fields which eliminates any negative contribution to the partition function. An approximation is then made to impose these constraints in the MC sampling to control the sign problem. We develop an algorithm to effectively carry out the MC sampling under the approximate formalism. We illustrate the method by applying it to the one-band Hubbard model. We show that accurate results, on both the energy and various correlation functions, can be obtained with the new method, even with simple forms of the approximate constraint.

The expectation value of a physical observable O is

$$\langle O \rangle = \frac{\mathrm{Tr}(Oe^{-\beta H})}{\mathrm{Tr}(e^{-\beta H})}, \tag{1}$$

where $\beta = 1/kT$ is the inverse temperature. The chemical potential term is implicit in the Hamiltonian H. The partition function in the denominator can be written as

$$Z \equiv \mathrm{Tr}(e^{-\beta H}) = \mathrm{Tr}[e^{-\Delta\tau H} \cdots e^{-\Delta\tau H} e^{-\Delta\tau H}], \tag{2}$$

where $\Delta\tau = \beta/L$ and L is the number of "time slices" on the right-hand side.

We next write the many-body operator $e^{-\Delta\tau H}$ in terms of single-particle operators. This is possible for most Hamiltonians or Euclidean actions of interest. For example, the Hubbard-Stratanovic transformation [4] can be applied for a Hamiltonian H which contains one- and two-body terms, denoted by K and V, respectively. This transformation replaces the two-body term $e^{-\Delta\tau V}$ by one-body interactions with a set of random external fields. Combining the result with the one-body term $e^{-\Delta\tau K}$, we can write

$$e^{-\Delta\tau H} \simeq \sum_{\mathbf{x}} B(\mathbf{x}), \tag{3}$$

where $\mathbf{x}$ denotes the random external auxiliary fields and $B(\mathbf{x})$ is a *single-particle operator*. The sum over all auxiliary fields recovers the interaction. For simplicity we have written the integration over $\mathbf{x}$ as a discrete sum. We have also suppressed spin indices, as well as the distribution function of $\mathbf{x}$. The approximation in Eq. (3) is from the Trotter error, which is of $\mathcal{O}(\Delta\tau^2)$ or less.

In the standard BSS formalism, Eq. (3) is substituted into Eq. (2). The trace over fermion degrees of freedom is then performed *analytically* [1,5], which yields

$$\mathrm{Tr}(e^{-\beta H}) = \sum_{X} \det[I + B(\mathbf{x}_L) \cdots B(\mathbf{x}_2) B(\mathbf{x}_1)], \tag{4}$$

where $X \equiv \{\mathbf{x}_1, \mathbf{x}_2, \ldots, \mathbf{x}_L\}$ denotes a complete path in auxiliary-field space. If the size of the single-particle

basis (e.g., number of spatial lattice sites) is N, the single-particle propagator $B(\mathbf{x}_l)$ is an $N \times N$ matrix and I is the corresponding unit matrix. The fermion determinant, which we will denote by $D(X)$, can be computed for each X. The sum over all paths can therefore be evaluated by MC methods. However, $D(X)$ is not always positive. As illustrated in Fig. 1a, the physical contribution comes from the small difference between the positive and negative components. The MC samples of X are drawn from the probability distribution defined by $|D(X)|$. As β increases, $D(X)$ approaches an antisymmetric function and its average sign vanishes exponentially. The variance in the MC estimate of Eq. (1) thus diverges, and the sign problem occurs.

A main obstacle to understanding and controlling the problem lies in the implicit and complex nature of the path-integral picture in this formalism. To gain insight, we return to the original form of Z in Eq. (2). We will use $\mathcal{B}$ to denote $e^{-\Delta\tau H}$ and imagine the following thought experiment to generate all possible auxiliary-field paths X. Beginning with $\mathrm{Tr}[\mathcal{B}\mathcal{B}\cdots\mathcal{B}\mathcal{B}]$, we substitute $\mathcal{B}$ with Eq. (3), one at a time from right to left. After l such steps, the partition function can be written as $\sum_{\{\mathbf{x}_1,\mathbf{x}_2,\ldots,\mathbf{x}_l\}} \mathcal{P}_l(\{\mathbf{x}_1,\mathbf{x}_2,\ldots,\mathbf{x}_l\},\mathcal{B})$, where P_l is

$$\mathcal{P}_l(\{\mathbf{x}_1,\mathbf{x}_2,\ldots,\mathbf{x}_l\},\mathcal{B}) \equiv \mathrm{Tr}[\underbrace{\mathcal{B}\mathcal{B}\cdots\mathcal{B}}_{L-l} B(\mathbf{x}_l)\cdots B(\mathbf{x}_2)B(\mathbf{x}_1)]. \quad (5)$$

As we proceed, we construct paths by including *all* possible values of $\mathbf{x}_l$. After L steps, all $\mathcal{B}$'s are replaced and all complete paths X are generated. Note that, while not the case in general, the trace in Eq. (5) can be performed when $l = L$, which, as expected, gives $D(X)$ of Eq. (4).

We now examine the procedure more closely, first at $\Delta\tau \to 0$, where $\mathcal{P}_l$ is continuous in l, the length of the partial path. In particular, we consider the case when $\mathcal{P}_l$ becomes zero for a certain partial path $\{\mathbf{x}_1,\mathbf{x}_2,\ldots,\mathbf{x}_l\}$. This means that, after the remaining $L-l$ steps have been finished, the sum over all possible configurations of $\{\mathbf{x}_{l+1},\mathbf{x}_{l+2},\ldots,\mathbf{x}_L\}$ will simply reproduce the $\mathcal{B}$'s in (5), leading to zero by definition. In other words, any complete path whose first l elements are $\{\mathbf{x}_1,\mathbf{x}_2,\ldots,\mathbf{x}_l\}$ is "noise"; the contributions of such paths cancel in Z. The signature of a noise path is $\mathcal{P}_l = 0$ for at least one l. Since $\mathcal{P}_0 > 0$, this shows that a complete path contributes if and only if the following L conditions hold:

$$\mathcal{P}_l(\{\mathbf{x}_1,\mathbf{x}_2,\ldots,\mathbf{x}_l\},\mathcal{B}) > 0, \qquad l = 1,2,\ldots,L. \quad (6)$$

If we impose the constraints in Eq. (6) in our procedure to generate the paths, we can eliminate all noise paths while selecting all contributing paths. The constraints are equivalent to having an absorbing boundary at the $\mathcal{P}_l = 0$ axis in Fig. 1b, thereby making the probability distribution of the generated complete paths vanish smoothly at the axis. This boundary condition (BC) eliminates complete paths that come in contact with the axis at any point, which cancels out the antisymmetric part of $D(X)$ in Fig. 1a. The algorithm remains exact.

At finite $\Delta\tau$, paths are discrete. But the BC is the same for the underlying continuous paths. To the lowest order in $\Delta\tau$, the constraints in Eq. (6) allow imposition of the BC under the discrete representation; the contact point ("triple point" in Fig. 1b) is approximated by the first l for which $\mathcal{P}_l < 0$. A higher order approach, which we use, is to interpolate between this l and $l-1$, with the probability to terminate at $l-1$ approaching 1 smoothly if $\mathcal{P}_{l-1} \to 0$ [6]. It is important to note that, in both approaches, the finite-$\Delta\tau$ error vanishes as $\Delta\tau \to 0$.

$\mathcal{B}$ is not known in practice. We replace it by a known trial propagator B_T. The constraints now yield approximate results, which become exact if B_T is exact. If B_T is in the form of a single-particle propagator, we can analytically evaluate the trace in Eq. (5) by making use of the same identity [5] that produced Eq. (4). The constraints in (6) can now be written as

$$\mathcal{P}_l^T = \det\left[I + \left(\prod_{m=1}^{L-l} B_T\right) B(\mathbf{x}_l)\cdots B(\mathbf{x}_1) \right] > 0 \quad (7)$$

for each l on $1 \le l \le L$, where we have introduced the shorthand $\mathcal{P}_l^T$ for $\mathcal{P}_l(\{\mathbf{x}_1,\mathbf{x}_2,\ldots,\mathbf{x}_l\},B_T)$.

The idea of the new method is then to generate MC samples of X which *both* satisfy the conditions in (7) *and* are distributed according to $D(X)$ [7]. To realize this efficiently, we construct the following algorithm, which builds directly into the sampling process both the constraints and some knowledge of the projected future contribution. In terms of the partial contributions $\mathcal{P}_l^T$, the fermion determinant $D(X)$ can be written as

$$D(X) = \frac{\mathcal{P}_L^T}{\mathcal{P}_{L-1}^T}\frac{\mathcal{P}_{L-1}^T}{\mathcal{P}_{L-2}^T}\cdots\frac{\mathcal{P}_2^T}{\mathcal{P}_1^T}\frac{\mathcal{P}_1^T}{\mathcal{P}_0^T}\mathcal{P}_0^T. \quad (8)$$

We construct the path X in L steps, corresponding to stochastic representations of the L ratios in Eq. (8). We start from $\mathcal{P}_0^T$, i.e., L B_T's in place of B's, with overall weight 1. Then, successively from $l = 1$ to L, we (a) pick an $\mathbf{x}_l$ from the conditional probability density function $p(\mathbf{x}_l \,|\, \mathbf{x}_{l-1},\ldots,\mathbf{x}_2,\mathbf{x}_1) > 0$ defined by $(\mathcal{P}_l^T/\mathcal{P}_{l-1}^T)/C$ and

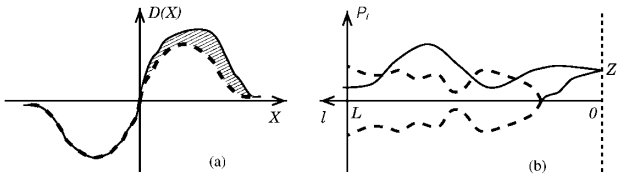

FIG. 1. Schematic illustration of the sign problem and the constraints to control it. Part (a) shows the integrand $D(X)$ of the partition function Z. The X axis represents an abstraction of the many-dimensional auxiliary-field paths X; each point denotes a collection of X's, e.g., in the sense of a bin in a histogram. In standard MC, $|D(X)|$ is sampled, while only the shaded area contributes. Part (b) shows $\mathcal{P}_l$ [Eq. (5)] as a function of the length of the partial path, l, for several paths. When $\mathcal{P}_l$ becomes 0, ensuing paths (dashed lines) cancel. Only complete paths with $\mathcal{P}_l > 0$ for all l (solid line) contribute in Z; they lead to the shaded area in (a).

(b) multiply the overall weight by the normalization factor $C \equiv \sum_{\mathbf{x}_l} \mathcal{P}_l^T / \mathcal{P}_{l-1}^T$. The algorithm allows $\mathbf{x}_l$ to be selected according to the best estimate of its potential contribution, reflecting the integrated (i.e., with dashed-line paths in Fig. 1b already canceled out) effect of all subsequent paths from $\mathbf{x}_l$. Note that the probability distribution for $\mathbf{x}_l$ vanishes smoothly as $\mathcal{P}_l^T$ approaches zero, and the constraints are naturally imposed.

We simultaneously propagate an ensemble of paths. The contribution of each path X in Z is given by its final weight. Given X, we can calculate both equal-time and (imaginary) time-dependent correlations through the single-particle Green's functions [5]. The expectation in Eq. (1) is a weighted average over X. The statistical accuracy improves as the procedure is repeated and more paths are generated.

We mention several technical issues. (i) We have chosen a noninteracting propagator, $e^{-\Delta\tau K}$, as B_T. More general mean-field propagators, including ones with imaginary-time dependence, can be incorporated straightforwardly. (ii) We divide each step for each path into substeps, in which we apply (a) and (b) to individual components of $\mathbf{x}_l$. This simplifies p and C (of the substeps) [1,6]. (iii) As paths are evolved, products of $B(\mathbf{x})$ and B_T must be stabilized against round-off errors [8]. (iv) The weights of paths fluctuate as they are propagated. We apply a population control mechanism [9] to improve efficiency. (v) Instead of using branching random walks to generate paths, it is possible to use a Metropolis scheme in which an overall acceptance-rejection procedure is applied after a potential complete path is proposed by sampling Eq. (8). We have not yet explored such a scheme. A detailed account of these and other algorithmic issues will be published elsewhere.

The algorithm we have described provides the *finite-temperature* counterpart of the *ground-state* constrained path Monte Carlo (CPMC) method [6]. The latter, which has been applied to study various lattice models, eliminated the sign decay in $T = 0$ K auxiliary-field calculations by constraining paths in Slater determinant space with a trial ground-state wave function $|\psi_T\rangle$ [6,10]. The chief difficulty in generalizing the concept of a constraining wave function or density matrix [11] to the finite-temperature formalism is twofold: (i) In this formalism, paths do not originate or end at the same point in Slater determinant space; different paths would thus require different constraining conditions. Indeed paths do not even have the same "dimension." (ii) With the analytical evaluation of the trace, the path-integral picture is implicit and would likely prevent implementation of such constraints. The new algorithm overcame the difficulty. It also provides a unified view of the zero- and finite-T algorithms. The constraining $|\psi_T\rangle$ in $T = 0$ K CPMC can be understood in terms of B_T operating on an arbitrary initial state.

We now apply the new algorithm to study the one-band Hubbard model. The model consists of interacting electrons on a square lattice. The Hamiltonian $H = K + V$ is given by $K = -t \sum_{\langle ij\rangle\sigma} (c_{i\sigma}^\dagger c_{j\sigma} + \text{H.c.}) - \mu \sum_i (n_{i\uparrow} + n_{i\downarrow})$ and $V = U \sum_i n_{i\uparrow} n_{i\downarrow}$, where $c_{i\sigma}^\dagger$ creates an electron of spin σ on site i, $n_{i\sigma} = c_{i\sigma}^\dagger c_{i\sigma}$ is the electron number operator, and $\langle\ \rangle$ indicates near neighbors. The on-site Coulomb repulsion is $U > 0$. In connection with high-T_c superconductivity, the Hubbard model has been the subject of intense theoretical effort for the past decade. The model provides a good test case, with both its challenging nature and the availability of certain benchmark data. Quantities of particular theoretical and experimental interest include the momentum distribution $n(\mathbf{k})$ and the d-wave electron pairing correlation $P_d(\mathbf{l})$ [12].

We study lattices of size $\sqrt{N} \times \sqrt{N}$ with periodic boundary conditions. The desired electron density $\langle n\rangle \equiv \langle \sum_{i\sigma} n_{i\sigma}\rangle / N$ is achieved by adjusting μ. Our trial propagator B_T is $e^{-\Delta\tau K}$ multiplied by $e^{-\Delta\tau\nu_T \sum_{i\sigma} n_{i\sigma}}$, where ν_T is a parameter. The second term in B_T accounts for $e^{-\Delta\tau V}$ in the sense of the restricted Hartree-Fock method.

In Fig. 2 and in Table I, we show results for a 4×4, $U = 4$ system where the sign problem is the most severe. This limits the range of temperatures where accurate calculations can be done with the standard algorithm. At $\beta = 12$, the average sign in BSS, $\langle s\rangle$, is projected to be less than 0.01 from the exponential decay rate [3] and the numbers in Table I; this β is thus not reachable by BSS with present computing power [15]. The system hence presents a challenging test case for the current algorithm. At high T, our algorithm gives results in excellent agreement with BSS results [14], which are exact. At low T, it

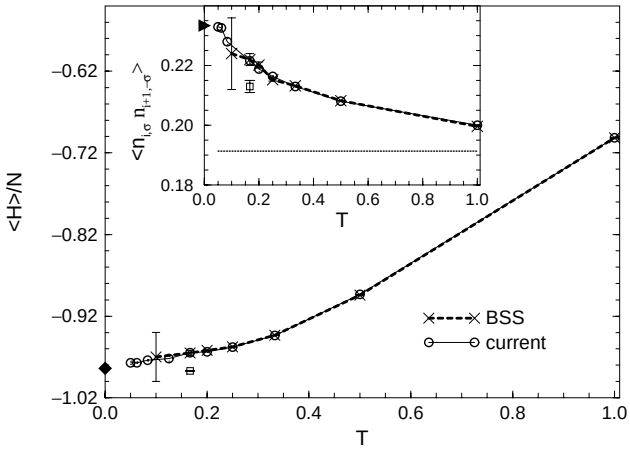

FIG. 2. Comparison with available data for a 4×4 system with $U = 4$ and $\langle n\rangle = 0.875$. The main graph shows the energy. The diamond at $T = 0$ is from exact diagonalization. The inset shows the density-density correlation function between near-neighbor sites. The algorithm accurately predicts the development of strong antiferromagnetic correlation as T decreases, despite the use of a constraining propagator B_T which by itself gives incorrect physics (flat line). At low T, the results converge to that of $T = 0$ K CPMC (triangle). Error bars in "current" are smaller than symbol size and are not shown [13]. BSS results are from Ref. [14]. For comparison, squares at $T = 0.1667$ show BSS results *with the sign neglected,* which is an uncontrolled approximation [3].

TABLE I. Further comparison of the current method with BSS and exact diagonalization (ED), on the same system as that of Fig. 2. $G(\mathbf{l})$ is the average Green's function $\langle c^{\dagger}_{i+\mathbf{l}\sigma} c_{i\sigma}\rangle$, and $P_d(\mathbf{l})$ the d-wave pairing correlation, at separation $\mathbf{l} = (l_x, l_y)$. The average sign in BSS is given by $\langle s\rangle$. In the last row, ED results are shown for G, while ground-state CPMC results are shown for P_d; the latter is *not* exact. Numbers in parentheses indicate statistical errors in the last digit.

β		$\langle s\rangle$	$G(1,0)$	$G(2,2)$	$P_d(2,1)$
3	Current		0.1631(1)	−0.0415(1)	0.0625(2)
	BSS	0.99	0.1631(1)	−0.0418(1)	0.0630(3)
6	Current		0.1663(3)	−0.0470(4)	0.077(2)
	BSS	0.44	0.1662(2)	−0.0465(2)	0.083(3)
20	Current		0.166(1)	−0.050(1)	0.078(2)
∞	Exact		0.167	−0.051	0.078(2)

reaches convergence and leads to results consistent with those from ground-state CPMC and in good agreement with those from $T = 0$ K exact diagonalization [16].

In Fig. 3, we show new results for an 8×8 lattice. The electron filling of $\langle n\rangle = 0.82$, which is in the physically relevant region, shows the worst sign problem, with $\langle s\rangle$ in BSS falling to ~ 0.1 at $\beta = 6$ [8]. Accurate and systematic calculations have therefore not been possible on this system. The new algorithm, on the other hand, required only modest computing time (about 2 days on a single processor of an SGI Origin200 workstation for $\beta = 16$) to reach the excellent statistical precision shown in the figure. As T decreases, the Fermi surface appears to contract along (π, π), while bulging along $(\pi, 0)$. The d-wave electron pairing correlation at large pair separations *increases* with decreasing T. The noninteracting system, however, also shows the same behavior. In fact, $P_d(\mathbf{l})$ in the latter is larger than the corresponding interacting

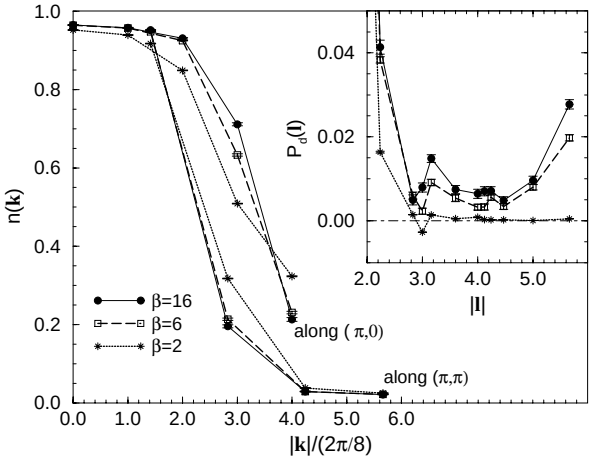

FIG. 3. Temperature dependence of the momentum distribution (main graph) and d-wave pairing correlation (inset) for an 8×8 system with $U = 4$ and $\langle n\rangle = 0.82$. [Recall $n(\mathbf{k})$ is the Fourier transform of $G(\mathbf{l})$.] As temperature $(1/\beta)$ lowers, the momentum distribution, shown along two directions in $\mathbf{k}$ space, becomes more anisotropic, and the long-range part of the d-wave pairing correlation increases.

results, consistent with results from ground-state CPMC [17]. More systematic calculations, at different $\langle n\rangle$, U, and system size, are currently being performed.

In summary, we have presented a quantum MC algorithm which allows finite-temperature, grand-canonical-ensemble simulations of fermion systems without any decay of sign. The method is approximate. We have shown that accurate results can be obtained with a simple constraining propagator B_T. An improved B_T will lead to improved results, and the method becomes exact when B_T is exact. The algorithm makes possible calculations under the field-theoretical formalism whose required computer time scales algebraically, rather than exponentially, with inverse temperature and system size. With the second-quantized representation, it complements the restricted path-integral MC method [11]. The algorithm automatically accounts for particle permutations and allows easy computations of both diagonal and off-diagonal expectations, as well as imaginary-time correlations.

I am grateful to R. T. Scalettar, M. Enjalran, and F. Assaad for providing benchmark data, and to J. Carlson for stimulating discussions. I thank D. L. Cox, R. L. Sugar, and J. W. Wilkins for helpful conversations, and the INT at the University of Washington for hospitality, where part of the work was done. This work was supported by the NSF under Grant No. DMR-9734041 and the Research Corporation.

[1] R. Blankenbecler *et al.*, Phys. Rev. D **24**, 2278 (1981); D. J. Scalapino and R. L. Sugar, Phys. Rev. Lett. **46**, 519 (1981).
[2] K. E. Schmidt and M. H. Kalos, in *Applications of the Monte Carlo Method in Statistical Physics*, edited by K. Binder (Springer-Verlag, Heidelberg, 1984).
[3] E. Y. Loh, Jr., *et al.*, Phys. Rev. B **41**, 9301 (1990).
[4] See, e.g., J. Hubbard, Phys. Rev. Lett. **3**, 77 (1959).
[5] J. E. Hirsch, Phys. Rev. B **31**, 4403 (1985).
[6] Shiwei Zhang *et al.*, Phys. Rev. Lett. **74**, 3652 (1995); Phys. Rev. B **55**, 7464 (1997).
[7] Note that the constraints in (7) ensure $D(X) > 0$, although the reverse is clearly not true.
[8] S. R. White *et al.*, Phys. Rev. B **40**, 506 (1989).
[9] C. J. Umrigar *et al.*, J. Chem. Phys. **99**, 2865 (1993).
[10] S. B. Fahy and D. R. Hamann, Phys. Rev. Lett. **65**, 3437 (1990).
[11] D. M. Ceperley, Phys. Rev. Lett. **69**, 331 (1992).
[12] The precise form we computed is $P_d(\mathbf{l}) \equiv \langle \Delta^{\dagger}_d(\mathbf{l}) \Delta_d(\mathbf{0})\rangle$, with $\Delta_d(\mathbf{l}) = \sum_{\boldsymbol{\delta}} f(\boldsymbol{\delta})\,(c_{\mathbf{l}\uparrow} c_{\mathbf{l}+\boldsymbol{\delta}\downarrow} - c_{\mathbf{l}\downarrow} c_{\mathbf{l}+\boldsymbol{\delta}\uparrow})$, where $\boldsymbol{\delta}$ is $(\pm 1, 0)$ and $(0, \pm 1)$, and $f(\boldsymbol{\delta})$ is 1 when $\boldsymbol{\delta} = (\pm 1, 0)$, and -1 otherwise.
[13] The curves show a small kink at $\beta = 6$, because at $\beta \leq 6$, the calculations were done at $\langle n\rangle$ matching that of the BSS calculations, which was larger than 0.875 (by $\sim 1\%$), while at $\beta > 6$, they were adjusted to give 0.875.
[14] R. T. Scalettar (private communication).
[15] E. Dagotto, Rev. Mod. Phys. **66**, 763 (1994).
[16] A. Parola *et al.*, Phys. Rev. B **43**, 6190 (1991).
[17] Shiwei Zhang *et al.*, Phys. Rev. Lett. **78**, 4486 (1997).